Aalborg Universitet

Aalborg University Denmark

Over-the-Air Testing for Connecting Faults Diagnosis in Beamforming Antenna Arrays with Short Measurement Distance

Li, Mengting; Franek, Ondrej; Zhang, Fengchun; Wang, Zhengpeng; Fan, Wei

Over-the-Air Testing for Connecting Faults Diagnosis in Beamforming Antenna Arrays with Short Measurement Distance

Mengting Li, Ondrej Franek, Fengchun Zhang, Zhengpeng Wang and Wei Fan

Abstract—A novel diagnosis method for detecting the connecting faults (i.e., disconnected and misconnected antenna elements) in beamforming antenna array is proposed. Compared with state-of-the-art methods, the proposed diagnosis method can be conducted when the phased array operates in its default beam-steering mode. Moreover, the proposed diagnosis method is fast since it only requires a few near-field measurement positions in a very short distance (i.e. the near-field of the array). Measurement uncertainties, e.g. the scatterings from the practical testing environment are considered in the method. Therefore, the proposed method can robustly detect beamforming array connecting faults in practical production line testing environments. The method is first validated using an 11-element dual-polarized base station antenna array at 2.7 GHz by numerical simulations. It is further experimentally validated using an 8-element single-polarized patch antenna array at 3.6 GHz. The same antenna array also serves as the probe array with only a 10 cm distance between the antenna under test and the probe array. The diagnosis results for different types of connecting faults with numerical simulations and measurement validations have verified the effectiveness and robustness of the proposed method in practical applications.

Index Terms—Over-the-air (OTA) testing, beamforming antenna array, array diagnosis, fault detection.

I. INTRODUCTION

Beamforming technology is adopted in communication systems to enhance the signal-to-noise ratio (SNR) [1]. Base stations (BSs) in long term evolution (LTE) systems have up to 5 arrays to support multi-band operation and each array might contain 8-11 dual-polarized antenna elements. The connecting faults are present due to the large number of antennas employed in the BSs and this issue becomes more pronounced as the number of elements gets even larger in sub-6 GHz 5G BS systems [2]. The connecting faults include disconnection faults caused by the degradation of related radio frequency (RF) components (i.e. antennas, cables and connectors), and misconnection faults caused by manual installation. For dual-polarized BS antennas, the connecting faults can be complex, which are related to three possible fault types, i.e. disconnected

antenna elements, swapped ports of antenna elements (for the same polarization), and swapped ports of two polarizations of the same antenna element. The first fault type is the same as failed elements detection in traditional array diagnosis methods [3]–[7]. Detecting the misconnection, i.e. the other two fault types, is also essential since it would affect the steering accuracy of the beamforming antenna.

The detection of connecting faults with assembled BS antennas in real-world production line environments can be very challenging in practice due to several reasons. 1) The assembled beamforming antenna is packaged in a radome and the inner antenna structures and feed ports are invisible from the outside. Over-the-air (OTA) testing [8], [9] where the device performance can be tested in a non-intrusive way is required. 2) The free control on phase or amplitude of individual array elements is not practical for assembled antennas. BS antennas with electric downtilt ability and switched beams are achieved by beamforming networks capable of generating some discrete pre-defined beam directions [10], [11]. 3) The testing solution should be fast to enable massive BS testing, which necessitates detection based on only a few measurement positions. 4) A robust method which can tolerate possible errors from non-ideal testing environments is preferred [12]. It would save much cost without the necessity of an RF clean environment, i.e. an anechoic chamber with almost no scatterings in the environment. However, it is non-trivial to overcome the above challenges.

Many efforts have been made to achieve array diagnosis. A well-known method is the backward transformation method (BTM) [3] using planar near-field data to obtain the far-field patterns of the array and then reconstruct the aperture field based on field transformation theory. However, a large number of samples (to satisfy Nyquist sampling theorem, i.e., the sampling interval can be generally selected as $\lambda/2$, where λ is the wavelength at the working frequency) and scanners with high accuracy are required, resulting in long measurement time and high cost. Another well-proven excitation reconstruction approach is the rotating element electric field vector (REV) method [4], [5], which relies on analyzing the power variation of the array signal while rotating the phase of antenna elements from 0° to 360° in turns. Matrix methods [6], [7] retrieve the excitations by solving linear systems relating the excitations to the field samples. A stable inversion of an ill-conditioned matrix can be obtained via a regularization strategy or other particular algorithms like the Landweber one. However, the required number of spatial samples for the matrix methods is

Mengting Li and Fengchun Zhang are with the Antenna Propagation and Millimeter-wave Systems (APMS) section, Aalborg University, Aalborg, Denmark.

Ondrej Franek is with the Department of Radio Electronics, Brno University of Technology, Brno, Czechia.

Wei Fan is with the National Mobile Communications Research Laboratory, School of Information Science and Engineering, Southeast University, Nanjing, China.

Zhengpeng Wang is with Electronics and Information Engineering, Beihang University, Beijing 100191, China.

Corresponding author: Wei Fan (Email: wfa@es.aau.dk).

much larger than the number of array elements to guarantee the estimation accuracy. In addition, the antenna element patterns should be known in advance to perform the inversion operation [7].

The difference between the excitations of a fault-free array and the antenna under test (AUT) can be solved using compressed sensing techniques [13]–[15] with a significantly reduced number of measurement samples. The number of the faulty elements should be much smaller than the number of the total elements in the AUT. The limitations are that the AUT element patterns and a faulty-free reference array should be known beforehand. Besides, the accuracy of the estimated excitations of the AUT elements might not be sufficient [15] for detecting any type of connecting faults, e.g., swapped ports between adjacent elements. The detection of the failure elements can also be successfully achieved by the artificial neural network (ANN) based techniques [16]–[18] with some pre-knowledge of the AUT. However, the ANN based techniques could suffer from the multiple local minima solutions, which might impair the diagnosis results. In [19], the array diagnosis could also be achieved by obtaining the excitations of the AUT elements based on assigning proper phase shift values on the AUT elements and solving the linear equations. A single probe is placed in the far-field of the AUT to receive the complex array response. However, dedicated phase tuning operations for individual elements are required, which is typically not supported by the production line testing. In [20], the calibration of the phased array is achieved by solving linear equations based on far-field measurement samples when the phased array working in its default beam-steering mode using the built-in phase shift settings. This method focuses on selecting the optimal set of beam-steering angles to accomplish the highest calibration accuracy. However, it is only effective for AUTs with powerful beam-steering capabilities, i.e., a wide scanning range and a sufficient number of scanning angles.

In this paper, a novel OTA testing method which can be conducted in a compact measurement setup when a BS antenna operates in its default beam-steering mode is proposed. The detection of faulty elements for various types of connecting faults is achieved by solving the relevant linear equations and implementing a differential strategy. The comparisons between the proposed method and several representative array diagnosis methods mentioned above are summarized in Table I. The attractive features of the proposed diagnosis method are listed as follows:

1) Default mode measurement. That is, the measurements can be conducted when the AUT, i.e. the beamforming antenna array, steers its beam to the pre-defined directions using the built-in phase shift settings.
2) Fast. All the antenna elements are diagnosed simultaneously with only a few measurement positions in the near field of the AUT. The whole diagnosis process could be completed in several minutes with the help of a fully automated measurement process.
3) Robust. The proposed method can be achieved in practical indoor or production line scenarios with possible scattering in the testing environment.
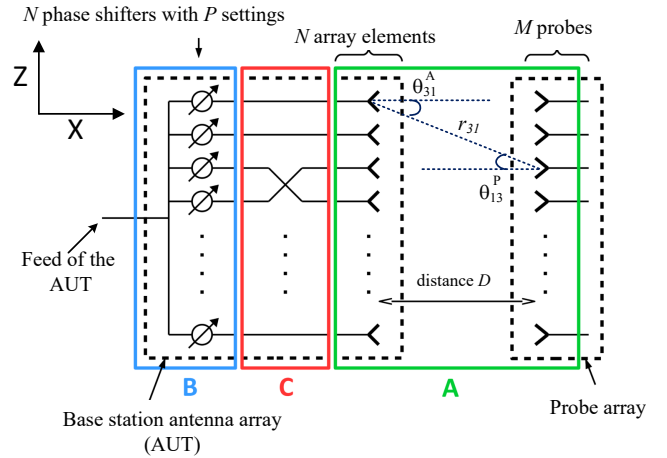

Fig. 1. Base station diagnostics system schematic.

This paper consists of five sections. The principle of the proposed detection method is described in Section II. Section III discusses the simulation results for a 1 by 11 dual-polarized linear beamforming antenna array. The algorithm is further verified by the measurements in Section IV. The conclusion is given in Section V.

II. METHOD

A. Signal Model

The schematic of the diagnosis setup is shown in Fig. 1. A beamforming antenna array including N antenna elements is on the left side enclosed by the black dashed line. The feed of the AUT is split into N branches with N phase shifters (one on each branch) connected to N antenna elements. The phase shifters can be set up with linearly progressing phase shifts to mimic the built-in phase shift settings of a BS beamforming array. Note that the phase shift settings are limited for several pre-defined steering beams as mentioned in the Introduction. The total number of phase shifter settings is P, allowing for steering the beam into P different directions. The schematic also depicts one of the fault types, in particular, the feeds of the 3rd and the 4th array elements are swapped, as an example. The probe array is on the right side of Fig. 1 also enclosed by the black dashed line. The proposed diagnosis method requires complex S-parameters (between the AUT feed on the left and the probe feed(s) on the right) at M different spatial locations. In practice, this could be achieved by either using a real probe array composed of M probe antennas connected to an M-path switch or using a virtual probe array i.e., moving a single probe antenna to M different locations with the help of a mechanical positioner. The former scheme is favorable for fast diagnosis since no mechanical movement is needed and the measurement process could be fully automated. Therefore, the real probe array with a switch is employed in our diagnosis system to reduce the measurement time. The distance between the AUT and the probe array is D. Fig. 1 shows only one polarization of the AUT and probe array. The other polarization follows the same arrangement, parallel to the depicted one.

The array diagnosis is based on the S-parameter received by M probes for P different phase shifter settings to detect

TABLE I
COMPARISONS BETWEEN THE PROPOSED METHOD AND THE STATE-OF-THE-ART WORKS.

Ref.	Key techniques	Number of the required spatial samples	Measurement distance	Limitations
[3]	Field transformation theory	$M^* \gg N^*$	Near-field	Long measurement time; high resolution scanner required
[7]	Matrix inversion with regularization strategy	$M \gg N$	Near-field	Long measurement time; knowledge of the AUT element patterns required
[15]	Differential strategy and compressed sensing technique	$M \ll N$	Near-field	Knowledge of the AUT element patterns and a faulty-free array required; limited capability of detecting different types of connecting faults
[19]	Matrix inversion with optimized condition number by designing phase shift setting matrix	$M = 1$	Far-field	Phase tuning of each element in the AUT required; large measurement distance
[20]	Matrix inversion with optimized condition number by selecting proper scanning angles	$M = 1$	Far-field	Applicable for AUT with at least N scanning angles and wide scanning range; large measurement distance
This work	Differential strategy and direct matrix inversion	$M \approx N$	Near-field	Knowledge of a faulty-free array required; applicable for AUT with at least 2 scanning angles

* M and N represent the number of the required spatial samples and the number of elements in the AUT, respectively.

any connecting faults in the AUT. The recorded S-parameter at a single frequency (measured as complex S_{21} by the vector network analyzer (VNA) in our measurements given in Section IV) can form a matrix $\mathbf{S} \in \mathbb{C}^{M \times P}$ with the (m,p)-th entry being the S-parameter between the feed of the AUT and m-th probe for the p-th phase shifter setting ($m \in [1,M]$, $p \in [1,P]$). Following Fig. 1, matrix $\mathbf{S}$ can be expressed as a matrix product of three matrices

$$\mathbf{S} = \mathbf{A} \cdot \mathbf{C} \cdot \mathbf{B} \tag{1}$$

where the matrices $\mathbf{A} \in \mathbb{C}^{M \times N}$, $\mathbf{C} \in \mathbb{Z}^{N \times N}$, and $\mathbf{B} \in \mathbb{C}^{N \times P}$ characterize three factors of the matrix $\mathbf{S}$. Namely:

- Matrix $\mathbf{A} = [a_{mn}]$ is the coupling matrix between the AUT element ports and the probe antenna ports. Its element a_{mn} represents the transmission coefficient between the ports of the n-th AUT element and the m-th probe antenna ($n \in [1,N]$). When the m-th probe is placed in the far-field of the n-th antenna element, the a_{mn} can be derived as [21]

$$a_{mn} = g_n(\theta_{mn}^A) \cdot g_m(\theta_{nm}^P) \frac{\mathrm{j}\lambda e^{-\mathrm{j}kr_{mn}}}{4\pi r_{mn}} \tag{2}$$

Note that the inter-element coupling is ignored here due to the typically negligible effects on the diagnosis results. Nevertheless, an AUT with strong inter-element coupling (unlikely for commercial base stations) could have an impact on the proposed diagnosis method. $g_n(\theta_{mn}^A)$ and $g_m(\theta_{nm}^P)$ are antenna field patterns for the n-th AUT antenna (in the direction of the m-th probe antenna with a view angle of θ_{mn}^A) and the m-th probe (in the direction of the n-th AUT antenna with a view angle of θ_{nm}^P), respectively. θ_{31}^A, θ_{13}^P and r_{31} are illustrated in Fig. 1, as an example. The fractional term on the right expresses the free-space path loss, where λ is the free-space wavelength, $k = 2\pi/\lambda$ is the wavenumber and r_{mn} is the distance between the n-th AUT element and the m-th probe antenna,

$$r_{mn} = \sqrt{D^2 + (z_m - z_n)^2} \tag{3}$$

where z_m and z_n are the z-coordinate values of the m-th probe antenna and the n-th AUT element, respectively with the z-axis being parallel to both linear arrays. The part of the diagnosis setup encompassed by matrix $\mathbf{A}$ is denoted by a green frame in Fig. 1.

- Matrix $\mathbf{B} = [b_{np}]$ is composed of P column vectors of complex excitation weights applied to the N antenna elements. Its single element b_{np} contains the complex excitation given to the n-th AUT element in the p-th phase shifter setting. One possible representation of $\mathbf{B}$ is

$$b_{np} = B e^{\mathrm{j}k(n - \frac{N+1}{2})\delta \sin \alpha_p} \tag{4}$$

where B is the magnitude weight for possible tapering, δ is the spacing between the AUT elements, and α_p is the target beam steering angle for the p-th phase shifter setting. In the following, $B = 1$, i.e. no tapering is assumed. The realm of matrix $\mathbf{B}$ is denoted by the blue frame in Fig. 1.

- Matrix $\mathbf{C}$ is the connection matrix between the phase shifters and the AUT elements. Matrix $\mathbf{C}$ is the diagonal matrix. Under normal circumstances, each phase shifter is connected to one antenna port and the $\mathbf{C}$ matrix is an identity matrix. However, if a fault occurs, this matrix is not an identity matrix anymore. For example, if n-th port is disconnected, then the corresponding diagonal element c_{nn} will be zero. If some ports are swapped, then the corresponding rows or columns in $\mathbf{C}$ will be swapped. The $\mathbf{C}$ matrix realm in Fig. 1 is denoted by the red frame.

It is the matrix $\mathbf{C}$ which gives us the information about accidental disconnections of some antenna ports or port swappings, and the structure of the matrix indicates which antenna ports are affected. Hence, to perform a successful diagnosis of the AUT, we need to determine matrix $\mathbf{C}$ with knowledge of matrix $\mathbf{S}$.

B. Proposed Beam-steering Diagnosis Method

1) Matrix Inversion: A diagnosis matrix $\mathbf{Q}$, i.e. a matrix that indicates the fault of the AUT, should therefore ideally be

matrix $\mathbf{C}$ from (1)

$$\mathbf{Q}_0 = \mathbf{C} = \mathbf{A}^{-1} \cdot \mathbf{S} \cdot \mathbf{B}^{-1} \qquad (5)$$

The $\mathbf{C}$ matrix can provide us with information of faulty elements as explained in Section II-A. Matrix $\mathbf{S}$ can be directly obtained by measuring transmission coefficients between AUT and the probe array, and matrix $\mathbf{B}$ is generally known as well following (4). However, matrix $\mathbf{A}$ is unknown and the approximation of matrix $\mathbf{A}$ and the inverse operation for both matrix $\mathbf{A}$ and $\mathbf{B}$ will introduce errors to the diagnosis system, as explained later. The accumulation of errors becomes large, making it impossible to obtain matrix $\mathbf{C}$ directly. To solve this problem, $\mathbf{A} \cdot \mathbf{C}$ or $\mathbf{C} \cdot \mathbf{B}$ can be employed as the updated diagnosis matrix, that is

$$\mathbf{Q}_1 = \mathbf{A} \cdot \mathbf{C} = \mathbf{S} \cdot \mathbf{B}^{-1} \qquad (6)$$

or

$$\mathbf{Q}_2 = \mathbf{C} \cdot \mathbf{B} = \mathbf{A}^{-1} \cdot \mathbf{S} \qquad (7)$$

For (6) or (7), only errors related to matrix $\mathbf{B}$ or $\mathbf{A}$ will be introduced to the system, respectively. The details will be discussed later in Section II-C. Successful fault diagnosis will then be achieved when we manage to detect zero rows (port disconnected) or swapped rows (ports swapped) from $\mathbf{Q}_1$ or when we can detect zero columns (port disconnected) or swapped columns (ports swapped) from $\mathbf{Q}_2$. As a consequence, we need to determine either $\mathbf{A}^{-1}$ or $\mathbf{B}^{-1}$.

Matrix $\mathbf{B}$ is known beforehand since we can calculate the complex excitations for each antenna from the known beam point and array configuration. Unfortunately, matrix $\mathbf{B}$ is a Vandermonde matrix by structure, and the condition number of these matrices is generally poor [20]. Thus, (7) is taken into consideration. Inverting $\mathbf{A}$ requires knowledge of the gain patterns of the antenna elements and the array configuration as in (2). From the geometrical arrangement of the array elements, we can determine distances r_{mn} and therefore the entire free-space path loss term. However, properties of the AUT elements, e.g. the antenna gain patterns in (2) cannot be known accurately since the radiation pattern of the antenna element in an array is different from the single isolated antenna pattern due to mutual coupling effects [22], [23].

Based on the described properties of $\mathbf{A}$ and $\mathbf{B}$, we have decided to choose (7), i.e. with inverting matrix $\mathbf{A}$. Since the exact $\mathbf{A}$ is unknown, an approximation $\mathbf{A}_{\mathrm{F}}$ containing only the free-space path loss term is used for inversion

$$a_{mn}^{\mathrm{F}} = \frac{\mathrm{j}\lambda \mathrm{e}^{-\mathrm{j}kr_{mn}}}{4\pi r_{mn}} \qquad (8)$$

This is equivalent to assuming that the gains of both the AUT elements and probes are equal to 1 (0 dB), i.e. both being omnidirectional. A related question is how to determine the number of the probes or spatial samples. In principle, a single spatial sample achieved by a single probe could be used in the proposed method when the radiation patterns of the AUT elements and the probe antenna are isotropic (i.e., the antenna radiates uniformly in all directions) or these antenna patterns are known beforehand. In these cases, the differences between

the matrix $\mathbf{A}$ and matrix $\mathbf{A}_{\mathrm{F}}$ can be eliminated. However, the ideal isotropic radiation patterns are not practical for the real-world AUT antenna elements and the radiation patterns of AUT elements are typically unknown. To make the proposed method practical, multiple spatial samples with a number of $M \approx N$ are required to guarantee that couplings with large signal powers in matrix $\mathbf{A}$ and matrix $\mathbf{A}_{\mathrm{F}}$ are similar. In this way, the impacts of the differences between matrix $\mathbf{A}$ and matrix $\mathbf{A}_{\mathrm{F}}$ can be mitigated and an accurate diagnosis can be finally achieved.

2) Differential Diagnosis: To achieve a more accurate and robust diagnosis, a differential approach has been taken. A reference array is introduced in the diagnosis system. This means that a difference is calculated between the diagnosis matrix of the actual AUT, i.e., $\mathbf{Q}$ and a diagnosis matrix of a reference AUT, i.e., $\mathbf{Q}^{(\mathrm{ref})}$. The compressed sensing based diagnosis techniques [13], [14] also employ a reference array and implement the differential strategy for diagnosis. However, the differential strategy in these techniques is used to transform the faulty elements diagnosis issue into a harmonic estimation of sparse signals. They rely on obtaining the excitations of the AUT to achieve diagnosis whereas the connecting faults detection using our proposed method is determined by the magnitude of the elements in matrix $\mathrm{d}\mathbf{Q}$ detailed as follows. From (7) the differential diagnosis matrix $\mathrm{d}\mathbf{Q}$ can be calculated as

$$\mathrm{d}\mathbf{Q} = \mathbf{Q}_2 - \mathbf{Q}_2^{(\mathrm{ref})} = (\mathbf{C} - \mathbf{C}^{(\mathrm{ref})}) \cdot \mathbf{B} = \mathbf{A}_{\mathrm{F}}^{-1} \cdot (\mathbf{S} - \mathbf{S}^{(\mathrm{ref})}) \quad (9)$$

Matrix $\mathrm{d}\mathbf{Q}$ indicates differences between the actual and reference AUTs as non-zero rows. On the other hand, rows corresponding to the AUT elements that work normally will be zero or close to zero. If we assume that the reference antenna is fault-free ("golden sample"), i.e. $\mathbf{C}^{(\mathrm{ref})} = \mathbf{I}$ (identity matrix), then the non-zero rows of $\mathrm{d}\mathbf{Q}$ indicate faulty elements of the AUT, and we have

$$\mathrm{d}\mathbf{Q} = (\mathbf{C} - \mathbf{I}) \cdot \mathbf{B} = \mathbf{A}_{\mathrm{F}}^{-1} \cdot (\mathbf{S} - \mathbf{S}^{(\mathrm{ref})}) \qquad (10)$$

3) Noise consideration: Considering the practical measurement environments and conditions in a production line, both $\mathbf{A}$ and $\mathbf{B}$ are perturbed by a uniformly distributed complex noise to evaluate the measurement uncertainties. This noise distribution is employed for simplicity since it is difficult to obtain the specific noise distribution for each noise source. Note that this distribution might not accurately account for the practical noise effects. However, the noise considerations here are used to provide initial insights on the robustness of the diagnosis system in the simulations. In particular

$$\tilde{\mathbf{A}} = \mathbf{A} + \gamma \max_{i,j} |a_{ij}| \mathbf{U} \qquad (11)$$

where $\mathbf{U}$ is a matrix of random complex numbers with real and imaginary parts uniformly distributed between -1 and $+1$, $\max |a_{ij}|$ is the largest magnitude of all elements in $\mathbf{A}$. Matrix $\mathbf{U}$ can be considered as a unit noise matrix. With this unit noise matrix, the ratio between the maximum signal power and additive noise power could be approximated by the coefficient γ. Similarly

$$\tilde{\mathbf{B}} = \mathbf{B} + \gamma \max_{i,j} |b_{ij}| \mathbf{U} \qquad (12)$$
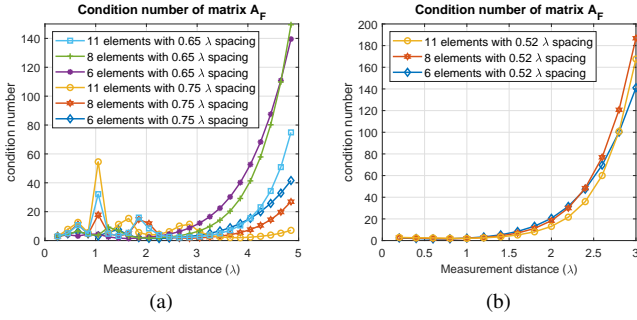
Fig. 2. The condition number of $\mathbf{A}_F$ for different array configurations.

The additive noise in matrix $\mathbf{A}$ accounts for the variant AUT antenna patterns and scattering in the measurement environment while the noise in matrix $\mathbf{B}$ simulates the uncertainty of the phase shifters. Furthermore, the noise in matrices $\mathbf{A}$ and $\mathbf{B}$ can contribute to the measurement noise in the probes as well.

S-parameters for the "golden array" (reference array) are calculated as

$$\tilde{\mathbf{S}}^{(\mathrm{ref})} = \tilde{\mathbf{A}}^{(1)} \cdot \tilde{\mathbf{B}}^{(2)} \tag{13}$$

whereas the faulty AUT measurement is represented by

$$\tilde{\mathbf{S}} = \tilde{\mathbf{A}}^{(3)} \cdot \mathbf{C} \cdot \tilde{\mathbf{B}}^{(4)} \tag{14}$$

where $\mathbf{C}$ is the connection matrix revealing the connecting faults, and the numbers in superscript denote different realizations of the random noise matrix $\mathbf{U}$.

The final diagnosis matrix is then

$$d\mathbf{Q} = \mathbf{A}_F^{-1} \cdot (\tilde{\mathbf{S}} - \tilde{\mathbf{S}}^{(\mathrm{ref})}) \approx (\mathbf{C} - \mathbf{I}) \cdot \mathbf{B} \tag{15}$$

where $d\mathbf{Q} = [q_{np}]$ of P column vectors representing the estimated connection situation of each array element with different scanning angles. A large value of $|q_{np}|$ indicates a big amplitude deviation of the n-th element between the AUT array and the "golden array", implying a potential connecting fault. More specifically, the connecting faults of the n-th element in the AUT can be determined by the magnitude of $|q_{np}|$ as shown below:

Case 1: $|q_{n1}| \approx |q_{n2}| \approx \cdots \approx |q_{nP}| \approx 0$
In this case, the n-th antenna element works correctly.

Case 2: $|q_{n1}| \approx |q_{n2}| \approx \cdots \approx |q_{nP}| \gg 0$
In this case, there is a disconnection fault or a misconnection of swapped ports for antenna element polarization on the n-th antenna element.

Case 3: $|q_{n1}| < |q_{n2}| < \cdots < |q_{nP}|$
In this case, there is a misconnection fault of swapped ports (for the same polarization) on the n-th antenna element.

Note that the $|q_{np}| > 0$ when the p-th phase shift setting does not correspond to $0°$ scanning angle for Case 3.

C. Discussions

1) Error Sources: In the proposed method, the accuracy of the diagnosis results will mainly be affected by two aspects.

The first factor is the condition number of matrix $\mathbf{A}_F$. A condition number for a matrix (i.e., matrix $\mathbf{A}_F$ in our case) measures how sensitive the answer is to the noisy data. It can be considered as an amplification factor of the noise or error in the system. As the condition number increases, the errors introduced by the inversion operation of the matrix $\mathbf{A}_F$ become more significant. The magnitude of $|q_{np}|$ for normal elements becomes large and these elements could be mistakenly interpreted as faulty elements. The condition number of matrix $\mathbf{A}_F$ depends on configurations of both the AUT and the probe array, and the measurement distance. Fig. 2 shows the condition number of matrix $\mathbf{A}_F$ under several typical BS array configurations as the measurement distance varies. Note that the probe number is the same as the element number of the AUT in this simulation. The condition number of matrix $\mathbf{A}_F$ is more sensitive to the element spacing of the AUT than the element number. Overall, it becomes larger as the measurement distance increases. A measurement distance, which is smaller than 2λ and 4λ can ensure a small condition number for an 8-element array with 0.52λ element spacing and an 11-element array with 0.65λ element spacing, respectively. This gives instructions on selecting the distance between the probe array and the AUT for the simulations and measurements in Section III and Section IV, respectively.

Another factor is the errors caused by the approximation of the real-world matrix $\mathbf{A}$. As discussed before, $\mathbf{A}_F$ considering only free-space transmission loss is used to replace matrix $\mathbf{A}$ in (10). There are mainly two aspects accounting for the differences between matrix $\mathbf{A}$ and $\mathbf{A}_F$. The AUT antenna element cannot be designed as an ideal omnidirectional antenna. A BS antenna element generally has a realized gain of 6-8 dBi. Thus, the transmission coefficients from real BS antenna elements to different probes will have a larger fluctuation range than an omnidirectional antenna. The distance between the AUT and probes will also have an impact on the approximation result because the realized gain of the AUT element in the direction of different probes varies greatly when the distance is small.

The paradox is that a long distance leads to a large condition number for matrix $\mathbf{A}_F$ yet a short distance introduces large differences between matrix $\mathbf{A}$ and $\mathbf{A}_F$. A trade-off is required for deciding the distance between the AUT and probe array to minimize the system errors. Fortunately, the proposed method focuses on detecting the faulty element(s) and fault type rather than retrieving the complex value of excitation for each antenna element, which is less sensitive to system errors and noise.

2) The Probe Array Configuration: The probe array configuration in terms of its aperture size and the number of probes will affect the diagnosis results. Generally, a larger aperture with more antenna elements can provide more information about the connection situations of the AUT. However, it will increase the errors caused by the approximation of matrix $\mathbf{A}$. The reason is that directional antennas are used in the AUT and probe array in reality, but omnidirectional patterns are assumed in our diagnosis method. A large probe aperture indicates a large field view angle of both the AUT and probe elements, which introduces more errors for our assumption. Moreover, too many probes placed in a fixed array aperture
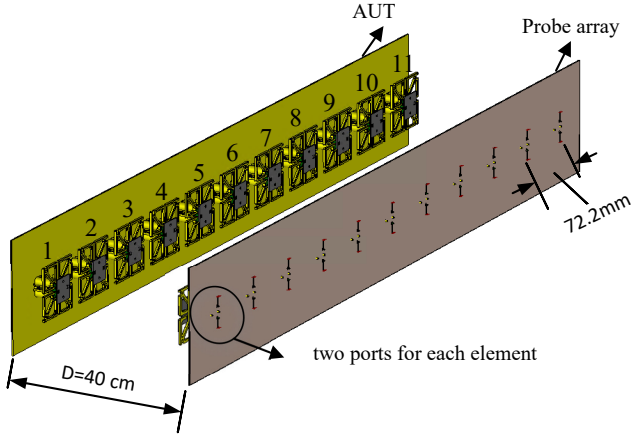
Fig. 3. The arrangement of the AUT and the probe array.

Fig. 4. The magnitude of (a) matrix $\mathbf{A}$ (left) and (b) matrix $\mathbf{A}_F$ (right).

will increase the mutual couplings between the antennas and scattering in the testing environment. On the other hand, sparse probe distribution or a small array aperture size of the probe array might not provide enough information of the whole AUT array.

A general guidance here is that the probe array has a similar aperture size and a similar number of elements to the AUT array. In this way, enough information about the connection situations can be obtained from the probes and significant errors caused by the approximation of matrix $\mathbf{A}$ can be avoided.

3) Limitations of the Proposed Method: In the proposed method, a reference array with no faulty elements is required to enable the differential strategy, which might not be easily available for all testing cases. Moreover, complex S-parameters between the reference array and the probe array, as well as between the AUT and the probe array, are required. However, accurate phase data are difficult to obtain for high frequency bands measurements. It also requires the port access of the AUT during the measurement, which might not be supported for future integrated radio systems. Finally, the proposed method is applicable to the AUT with built-in beam-steering capability. Measurements with at least two different scanning angles can achieve the diagnosis purpose. However, more scanning angles might be required to gain confidence in the diagnosis results.

III. NUMERICAL VALIDATIONS

In the following, simulations in CST Microwave Studio have been conducted to obtain the S-parameters of the reference array i.e., matrix $\tilde{\mathbf{S}}^{(\mathrm{ref})}$ and the numerical simulations in Matlab are used to validate the whole diagnosis process.

A. Simulation Environment

An 11-element beamforming antenna array shown in Fig. 3 serves as the AUT in our simulation. The antenna element is a $\pm45°$ polarized antenna operating at 2.7 GHz. This array has a total of 22 ports, with 11 ports for each polarization. The element spacing is set as 72.2 mm (0.65λ at 2.7 GHz). The beam can be steered from 0° to 15° with a step of 3°. The array
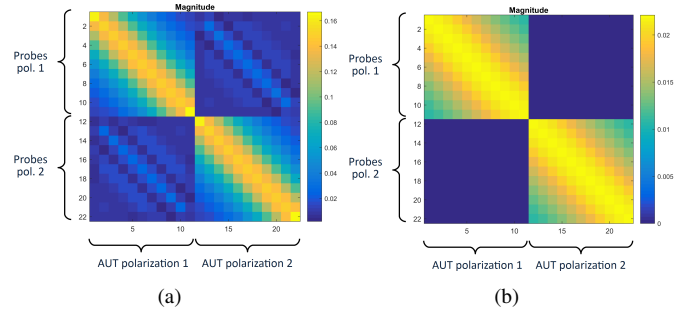
in Fig. 3 is used for validating the diagnosis method, but the method is not limited to this particular type and arrangement of the array elements. The fault types are detected by a linear array of probes arranged opposite the AUT. The probes should be dual-polarized in the same directions as the AUT. In our simulations, the AUT and the probe array are composed of the same antenna elements. However, the probe antenna types can be different in production units. Note that the probe array is not a phased array since each antenna element port should be accessible in the proposed method. The investigated scenario is shown in Fig. 3. The distance between the AUT array and probe array is selected as 40 cm (around 3.6λ) to obtain small system errors based on the discussions in Section II-C. Matrix $\mathbf{A}$ is a matrix of transmission coefficients between the AUT and probes at 2.7 GHz obtained from simulation results using CST Microwave Studio. The simulation results for different types of connecting faults are given in Section III-C 1)-4) to demonstrate the effectiveness of the proposed method. The effects of the noise level and the reduced size of the probe array are also explored in Section III-C 5) and 6), respectively. Note that a conservative noise level, i.e., $\gamma = 0.02$ is used for simulations in subsections 1), 2), 3), 4) and 6) whereas $\gamma = 0.01$ and $\gamma = 0.04$ are also considered for simulations in subsection 5).

B. Algorithm Performance Analysis

The structure of matrix $\mathbf{A}$ for the investigated diagnosis setup is shown in Fig. 4 (a). The two diagonal 11×11 submatrices represent the co-polarization coupling between the two arrays, whereas the two off-diagonal submatrices represent the cross-polarization coupling. Matrix elements on the main diagonal are the strongest in magnitude and express the boresight coupling between the corresponding opposite elements of the AUT and probe arrays as shown in Fig. 4 (a). Fig. 4 (b) shows the magnitude of $\mathbf{A}_F$ which serves as an approximation for $\mathbf{A}$ to be inverted. The maximum value of the magnitude is much smaller than that in matrix $\mathbf{A}$ due to the 0 dB gain set for both the AUT elements and the probe antennas. The diagonal elements are still the strongest, but not so pronounced, because (8) does not contain the gain terms and thus acts as a coupling matrix of omnidirectional antennas.
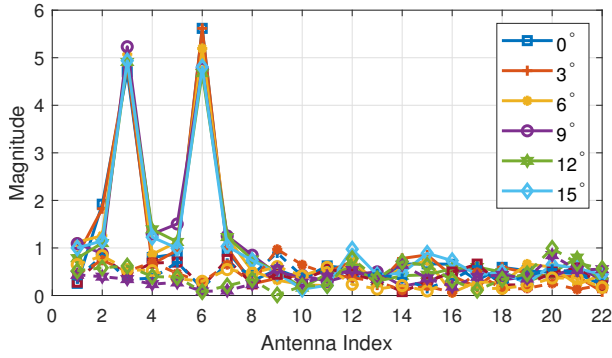
C. Simulation Results

Since different array elements have different electromagnetic conditions, an antenna near the edge (element 3) and
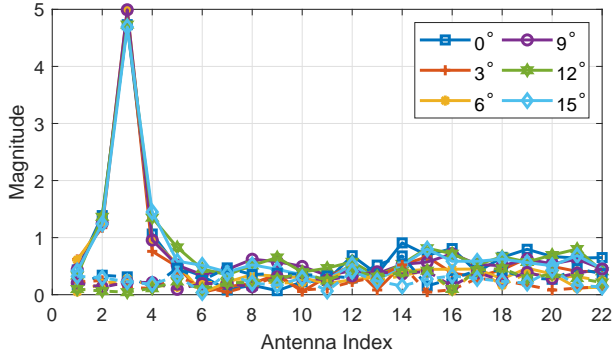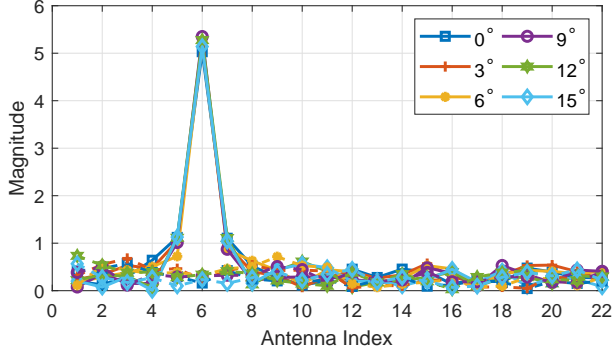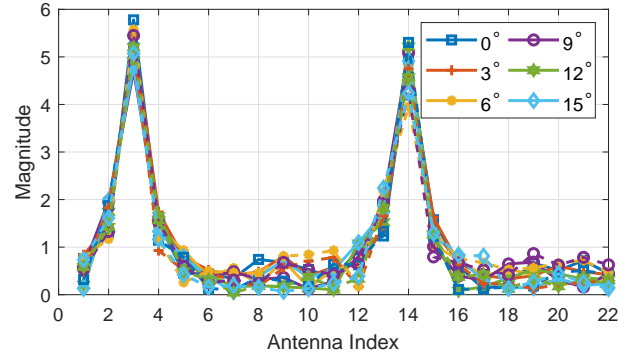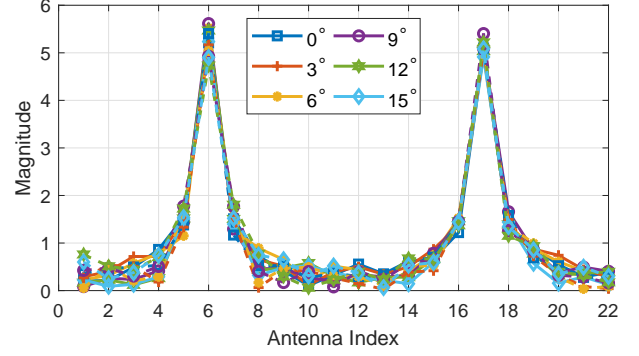
Fig. 5. The magnitude of elements in dQ when (a) element 3, (b) element 6, (c) both elements 3 and 6 are disconnected, respectively (solid lines for the first polarization and dashed lines for the second polarization).
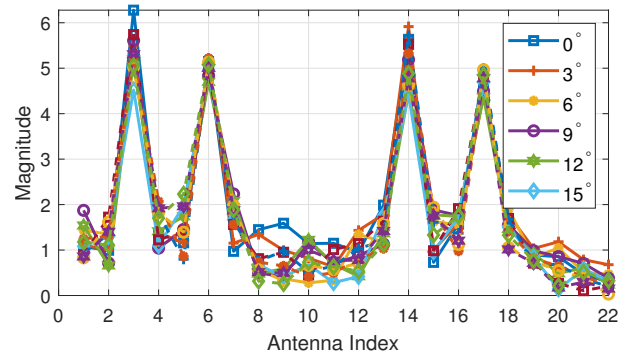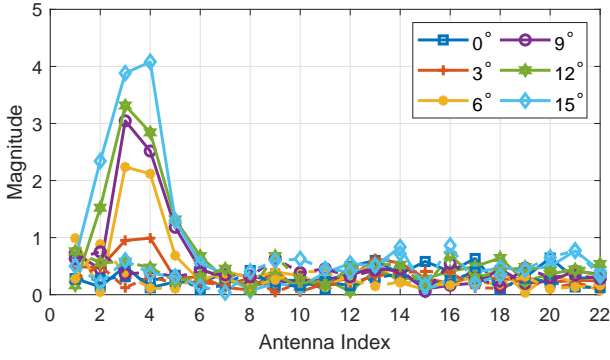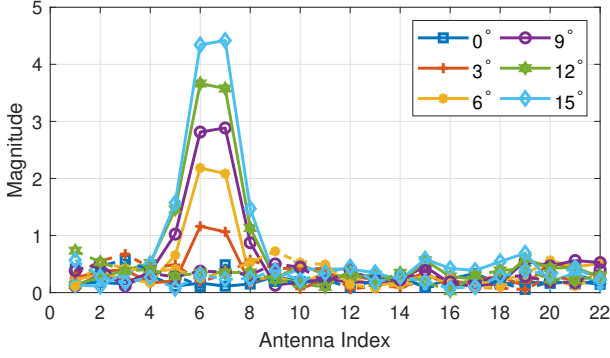

Fig. 6. The magnitude of elements in dQ when the polarization ports of (a) element 3, (b) element 6, (c) both elements 3 and 6 are swapped, respectively (solid lines for the first polarization and dashed lines for the second polarization).

a center antenna (element 6) are chosen as examples to investigate different connecting fault types. As discussed, the number of the probes is the same as the AUT antenna element number to obtain optimal diagnosis results. Antenna indices 1–11 represent the first polarization of elements 1–11 and the other polarization is given by indices 12–22. In the diagnosis results shown below, each curve represents the magnitude of a column in the diagnosis matrix for a specific scanning angle, which corresponds to a specific phase shift setting. Note that the diagnosis requires at least two different scanning angles to detect the faulty elements and distinguish the type of connecting faults. However, more diagnosis results from different scanning angles help us gain confidence in achieving a successful and accurate array diagnosis.

1) Disconnected Antenna Elements: This fault type shows the disconnection faults. Fig. 5 (a) and (b) show the magnitude of dQ when element 3 or element 6 is disconnected, respectively, whereas Fig. 5 (c) shows the results when two elements (i.e., both element 3 and element 6) are disconnected simultaneously. Obvious peaks appear at the indices of disconnected elements indicating successful detection. The diagnosis curves of different scanning angles have very small differences in this case since there is no or low level signals on the RF paths of the disconnected elements for all scanning angles.
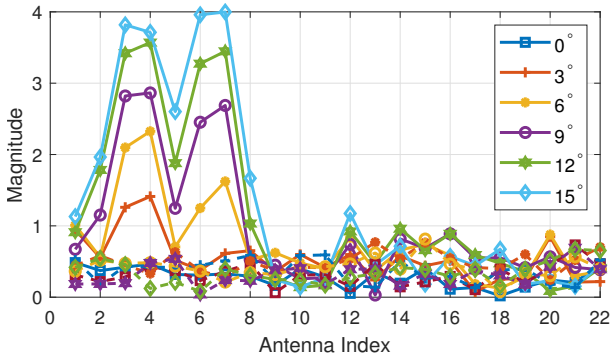
2) Swapped Ports for Antenna Element Polarization: This fault type represents misconnection cases, i.e. swapped ports of two polarizations of the same antenna element. High peaks appear at antenna indices 3 and 14 as shown in Fig.
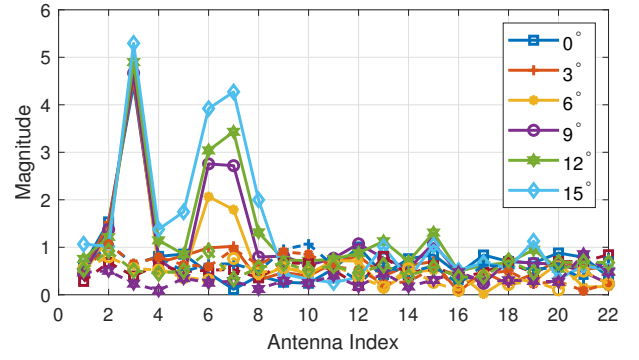
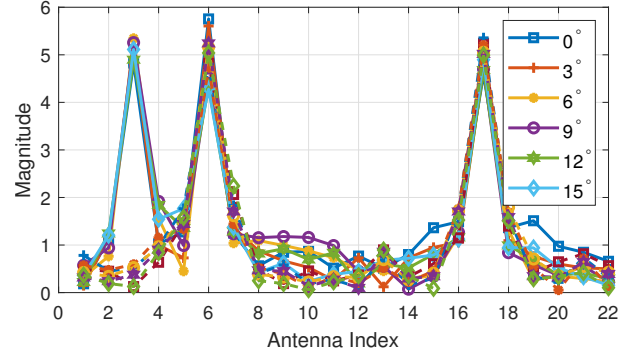Fig. 7. The magnitude of elements in dQ when ports (of the same polarization) between (a) elements 3 and 4, (b) elements 6 and 7, (c) both elements 3 and 4, elements 6 and 7 are swapped, respectively (solid lines for the first polarization and dashed lines for the second polarization).

Fig. 8. The magnitude of elements in dQ when (a) element 3 is disconnected, and ports of elements 6 and 7 are swapped, (b) element 3 is disconnected, and polarization ports of element 6 are swapped, (c) polarization ports of element 3, and ports of elements 6 and 7 are swapped, respectively (solid lines for the first polarization and dashed lines for the second polarization).

6 (a) indicating that there are connecting errors with two polarizations of element 3. Similar detection results can be seen in Fig. 6 (b) and (c).
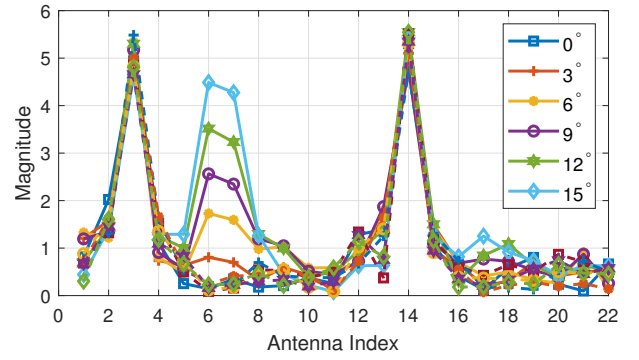
3) Swapped Ports of Adjacent Elements (for the Same Polarization): The third connecting fault type represents another misconnection case, which is the most challenging one, especially for the neighboring antenna elements. The amplitude of the signal fed to the neighboring elements is almost the same. Thus, the difference between the AUT array and the "golden array" is mainly caused by the phase, which is determined by the scanning angle. The detection results for single misconnection cases are shown in Fig. 7 (a) and (b) for element 3 and element 6, respectively, whereas double misconnection case (i.e., both element 3 and element 6) is

given in Fig. 7 (c). The peaks at indices of faulty elements progressively rise as the scanning angle becomes larger due to the increasing phase difference. However, the peaks at indices of faulty elements will be almost the same for all scanning angles when the fault type is disconnected antenna elements as we discussed before. The diagnosis results from different scanning angles are necessary since they help us gain more confidence in identifying the faulty elements and the fault type.

4) Mixed Connecting Faults: This type of connecting fault represents the cases when different types of connecting faults mentioned above appear simultaneously. Fig. 8 shows the different mixed connecting faults on elements 3 and 6. The results show that all the connecting faults can be success-

fully detected, which further verifies the effectiveness and accuracy of the proposed method. Note that the method should be capable of detecting other connecting faults, such as disconnection of an arbitrary number of elements, ports of the same polarization, and different polarizations swapped between arbitrary elements, since the working principle is the same.

5) Noise Effects: Two common types of connecting faults, i.e., disconnected antenna element and swapped ports of adjacent elements (for the same polarization) are employed to explore the noise effects with different value of γ in (11) and (12). Fig. 9 (a), (b) and Fig. 5 (a) show the diagnosis results when element 3 is disconnected with $\gamma = 0.01$, 0.04 and 0.02, respectively. Fig. 9 (c), (d) and Fig. 7 (a) show the diagnosis results when ports (of the same polarization) between elements 3 and 4 are swapped with $\gamma = 0.01$, 0.04 and 0.02, respectively. As the value of γ increases, a higher power level of noise will be introduced into the diagnosis system. For both types of connecting faults, the magnitudes for the fault-free antenna elements have larger variation ranges with a higher value of γ. For the disconnection case, obvious peaks appear at the index of the faulty element even with the γ of 0.04. The detection of the swapped ports case becomes more difficult with small scanning angles as the value of γ increases although successful diagnosis can still be achieved by analyzing the results from all the scanning angles. Measurements with large scanning angles are favorable for diagnosis in very noisy environments.

6) Effects of Reduced Number of Probes: As discussed in Section II-C, a reduced number of probe antennas might not provide enough information for achieving an accurate diagnosis of the AUT. The connecting fault types of disconnected antenna elements and swapped ports of adjacent elements (for the same polarization) are considered as examples. In Fig. 10, the number of the probe antennas is reduced from 11 to 6 and the 6 probes are selected from the previous 11-element probe array with an equal element spacing which is twice of the original element spacing. Fig. 10 (a) and (b) show the diagnosis results using 6 probes for disconnected antenna element case and swapped ports of adjacent elements case, respectively. Compared with the results shown in Fig. 5 (a), Fig. 10 (a) has false peaks at the indices of the first polarization of elements 5, 8 and 9 which could result in wrong detection of the faulty elements. Compared with the results shown in Fig. 7 (a), the false peaks can be clearly observed at the indices of elements 8 and 9 in Fig. 10 (b). Therefore, for an AUT composed of N antenna elements, around N probe antennas or spatial samples are required to guarantee the accuracy of the diagnosis results.

IV. MEASUREMENT VALIDATION

A. Measurement Setup

A preliminary measurement system was built in a laboratory environment at Aalborg University to validate the proposed method, as illustrated in Fig. 11, and the details of the included components are shown in Table II.

In the measurement, the diagnosis for an eight-element single-polarized linear array was demonstrated for simplicity.
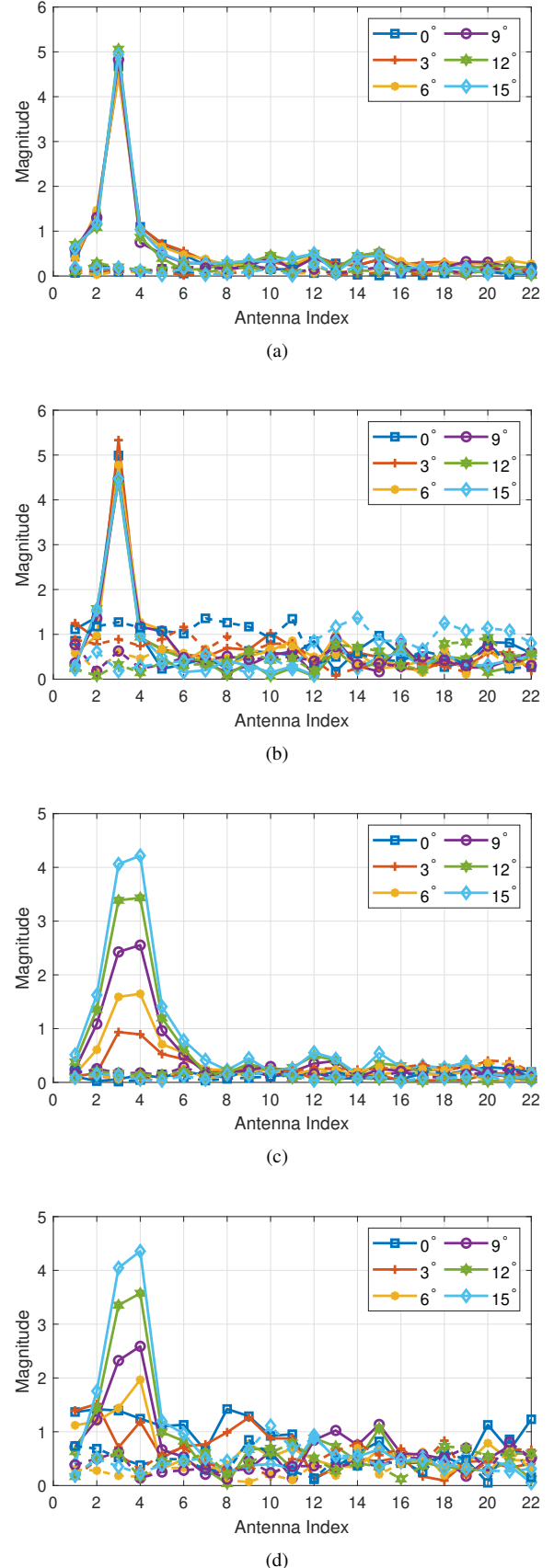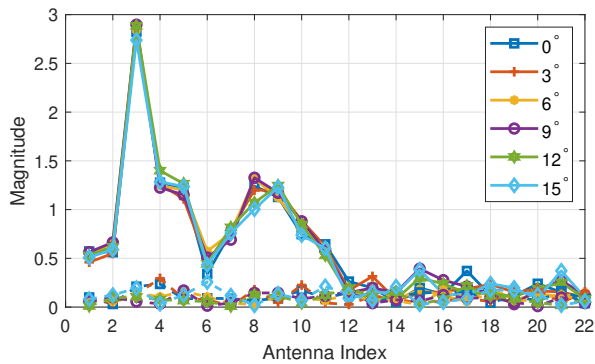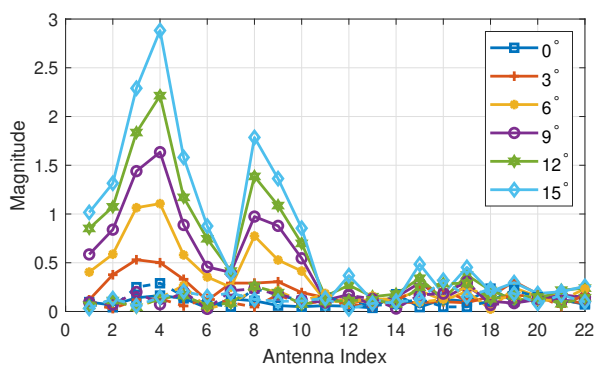

(a)

(b)

(c)

(d)

Fig. 9. The magnitude of elements in d**Q** (a) when element 3 is disconnected with γ=0.01 and (b) γ=0.04, respectively and (c) when ports (the same polarization) between elements 3 and 4 are swapped with γ=0.01 and (d) γ=0.04, respectively (solid lines for the first polarization and dashed lines for the second polarization).

(a)

(b)

Fig. 10. The magnitude of elements in $\mathrm{d}\mathbf{Q}$ using 6 probe antennas when (a) element 3 is disconnected and (b) ports (the same polarization) between elements 3 and 4 are swapped, respectively (solid lines for the first polarization and dashed lines for the second polarization).
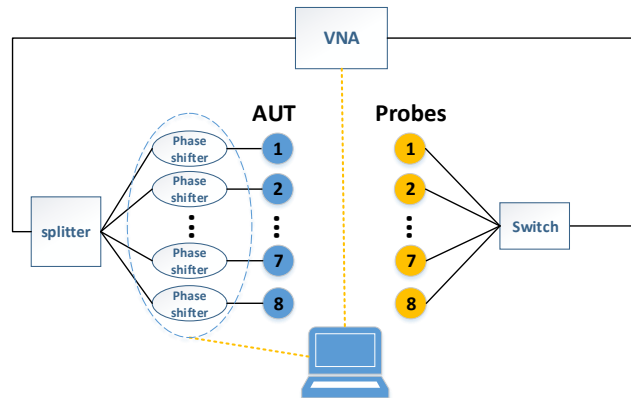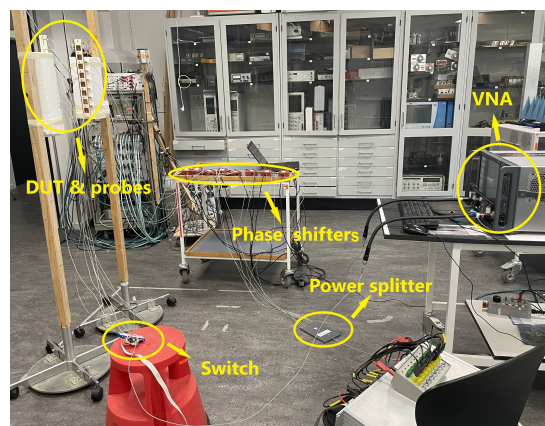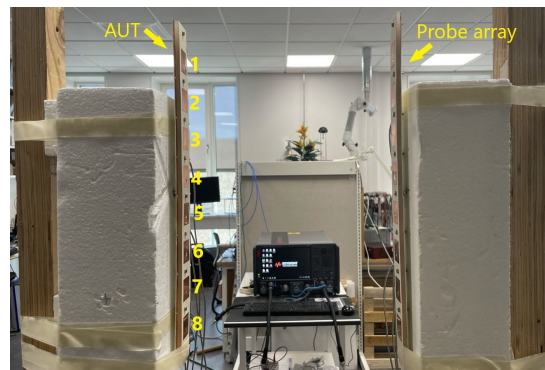

Fig. 11. An illustration of the measurement system.

(a)

(b)

Fig. 12. Photographs of (a) measurement system and (b) configuration of the AUT and probe antennas.

TABLE II
MEASUREMENT SYSTEM COMPONENTS AND SETTINGS

Component	Setup and specifications
VNA	• Model: Keysight N5227B • Measurement frequency: 3.6 GHz
Digital phase shifters	• Model: Vaunix Lab Brick LPS-402 • Frequency: 2–4 GHz • Adjustment range & resolution: 360° ; 1°
AUT and the probe array	• Antenna type: 1×8 single-polarized patch array antennas • Array dimensions: 35 mm × 380 mm × 5 mm • Element spacing: 43 mm • Realized gain: 5.5 dBi at 3.6 GHz
8-way power divider	• Model: Pulse Microwave PS8-12-454 • Frequency Range: 0.5–6 GHz
Switch	• Model: American Microwave Corporation MSR-8 DR-DT
Computer	• The computer is used to control the phase shifters and communicate with the VNA.

Note that the diagnosis method proposed in Section II can be applied to a larger scale array with dual-polarized antenna elements and arbitrary array configuration in principle. The measurement data were recorded at 3.6 GHz, which is the center frequency of the AUT. The AUT and the probe antennas are aligned, numbered and set face-to-face as shown in Fig. 12 (a). In our measurement, the distance between the AUT and the probe array was chosen as 10 cm (around 1.2λ) as a trade-off between the condition number of matrix $\mathbf{A}$ and the errors

introduced by the AUT radiation pattern approximation. The antennas were set at a height of 150 cm. In our measurement setup, the VNA is used to record the S-parameters. However, other measurement devices which can also obtain the S-parameters could be alternatives, e.g. the signal generator and the signal analyzer together with a coupler or calibration cable. In the measurements, the signals generated by the VNA were fed into the power splitter, phase shifted by the digital phase shifters, and then radiated by the AUT. The array complex signals received by the probe antennas were sequentially recorded by the VNA. An 8-path switch was employed to obtain the array signal data for each probe antenna by turns. The phase difference introduced by connecting lines and power dividers on each path was calibrated. The phase difference was within $[-0.6°, 0.6°]$ after the calibration. The amplitude deviation for different paths was within $[-0.15 \text{ dB}, 0.15 \text{ dB}]$, which is negligible. Note that the measurements do not require a strictly clean RF environment. The validation measurements can be completed in an indoor environment as shown in Fig. 12 (b), which is essential to reduce system cost.

To validate the diagnosis algorithm, two sets of measurements were conducted. For the first measurement, the AUT was set in a "fault-free mode", which means no connecting faults exist in the AUT array. This measurement is designed for obtaining the "golden sample" (S_0). For the second measurement, a certain fault type occurs within the AUT. Note that swapped connection between two polarization ports of the same antenna element case cannot be validated in the measurement session, since both the AUT and the probe antennas are single-polarized. To reduce the measurement time, only disconnection faults: elements 1 or 4 disconnected, and misconnection faults: elements 1 and 2 swapped and elements 4 and 5 swapped were measured. The steering range was set within $[0°, 15°]$, with a step of $3°$. For each measurement campaign, the array complex signals received by each probe under different scanning angles were measured.

B. Measurement Results

1) Analysis of Matrix $\mathbf{A}$ and $\mathbf{A}_F$: Fig. 13 shows the magnitude of matrices $\mathbf{A}$ and $\mathbf{A}_F$. It is reasonable that the maximum value was obtained when the antenna element and the probe were placed face to face. Comparing Fig. 13 (a) and (b), it can be noticed that the curves of matrices $\mathbf{A}$ and $\mathbf{A}_F$ have the same variation trend whereas matrices $\mathbf{A}$ has a larger dynamic range. The reason is that the magnitude of matrix $\mathbf{A}_F$ varies only due to different free-space pathloss caused by different distances between the antenna elements of the AUT and the probe array, whereas the magnitude variation of matrix $\mathbf{A}$ also includes the effects of radiation patterns. Although there are some differences between matrix $\mathbf{A}$ and $\mathbf{A}_F$, the variation trend is similar for the magnitude of the matrices.

2) Disconnected Element: Element 1 and element 4 were used as examples to verify the feasibility of the proposed method for edge and center antenna elements, respectively. The diagnosis results for disconnected element fault type are shown in Figs. 14 and 15. The magnitude of the differential
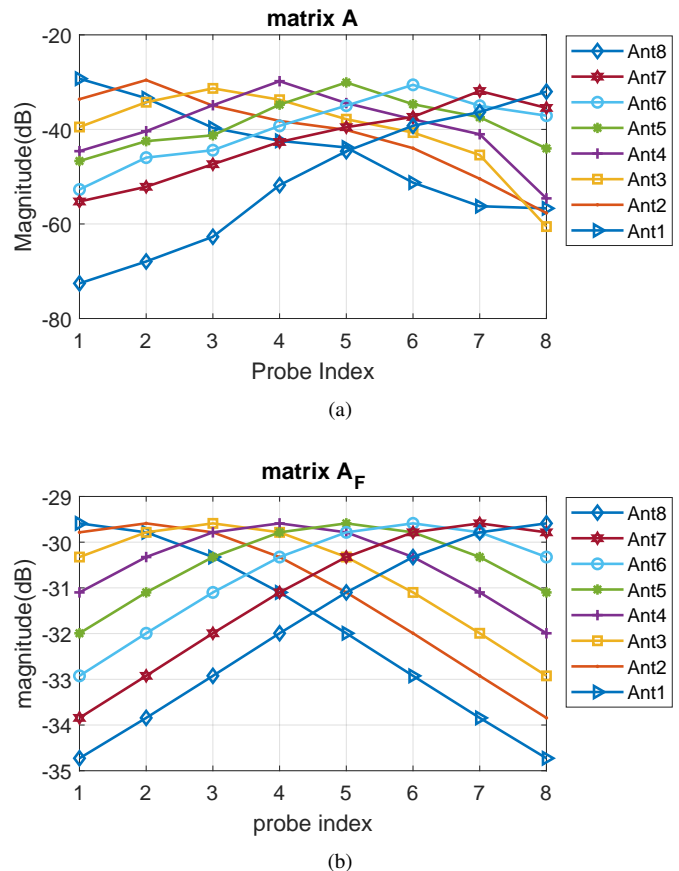

Fig. 13. The magnitude of matrices (a) $\mathbf{A}$ and (b) $\mathbf{A}_F$.
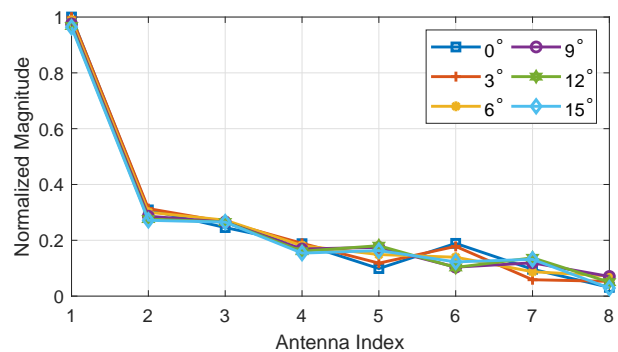

Fig. 14. The magnitude of the differential diagnosis matrix $\text{d}\mathbf{Q}$ for fault type of element 1 disconnected.
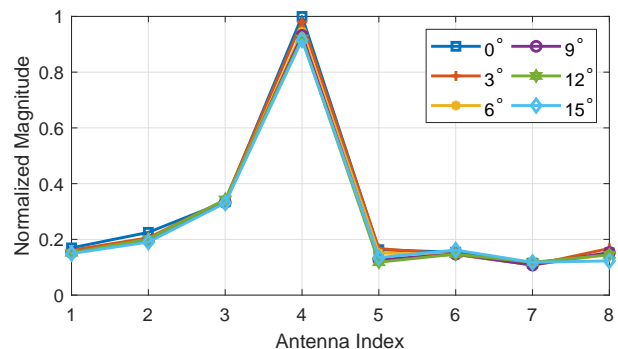

Fig. 15. The magnitude of the differential diagnosis matrix $\text{d}\mathbf{Q}$ for fault type of element 4 disconnected.
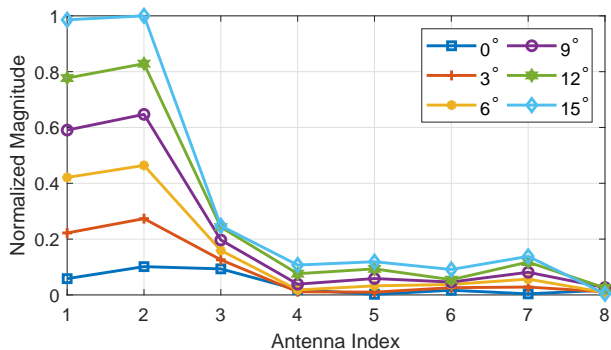
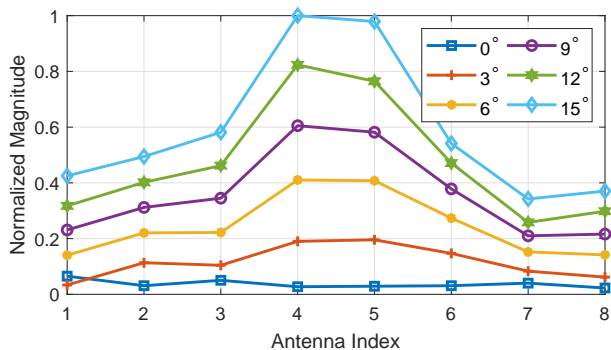Fig. 16. The magnitude of the differential diagnosis matrix d**Q** for fault type of elements 1 and 2 swapped.

Fig. 17. The magnitude of the differential diagnosis matrix d**Q** for fault type of elements 4 and 5 swapped.

diagnosis matrix d**Q** was normalized to 1 for clarity. It is clear that the element disconnected faults can be easily detected for both the edge element and the inner element. An obvious peak appears at the disconnected antenna index for all scanning angles.

3) Swapped Ports of Adjacent Elements: The diagnosis results for ports swapped detection is more sensitive to the measurement distance or relative positions of the AUT and the probe array compared with the disconnected mode, which makes it more difficult to detect the faults. As seen in Fig. 16, the swap between two edge elements, i.e., elements 1 and 2, can be recognized when the scanning angle is not $0°$. The value of $|q_{np}|$ is around 0 for all elements when the scanning angle is $0°$. The reason is that the swapped elements have almost the same excitations making it hard for probes to detect the excitation differences when the beam of the AUT array points in the boresight direction. It is reasonable to eliminate the $0°$ diagnosis result in this fault type, because the results will naturally be the same due to identical phase shifts. The employment of multiple scanning angles can help us identify the correct detection in the whole diagnosis results as discussed in III-C. The peaks at the indices of faulty elements become more obvious as the scanning angle becomes larger since the larger scanning angle provides larger phase differences for adjacent elements. The results for swapped ports of inner elements, i.e. elements 4 and 5, are shown in Fig. 17. Except for the boresight case, the ports swap between elements 4 and 5 can be successfully detected.

The measurements demonstrate that the proposed method is viable for base station antenna diagnosis applications. Besides, the measurement distance is only 10 cm between the AUT and the probe array and no RF clean environment is required. The diagnosis can be achieved in a very compact and non-ideal indoor measurement environment, making it a promising choice for the industry.

V. Conclusion and Future Work

In this paper, a novel diagnosis method based on the measurement of S-parameters between the AUT and a probe array is proposed for connecting faults detection in beamforming antenna arrays. Generally, the probe array which is the same as the AUT, and a short measurement distance between the AUT and the probe array can be used for both simulation and measurement validations. The proposed method works for a beamforming antenna array operating in its default beam-steering mode. The diagnosis method assisted by a differential approach is provided and validated numerically and experimentally. Simulation and measurement results indicate that the diagnosis accuracy can be affected by the number of probes, the scanning beams as well as the measurement distance between the AUT and the probe array. The proposed method will have a promising application for array diagnosis in real-world production line environments. Successful diagnosis can be achieved without phase shift control on individual antenna elements and only a few near-field data samples. Moreover, all the measurements can be conducted in a practical testing environment without the need for an ideal RF clean environment.

In addition to all the merits provided by the proposed method, there are also some limitations. The measurement distance should be carefully selected as a balance between the condition number of the matrix $\mathbf{A}_F$ and the approximation accuracy of matrix $\mathbf{A}$. As a result, it might take several measurement trials to determine the optimum measurement distance between these two arrays to achieve minimum system errors. Besides, it would be very beneficial and useful if a detection threshold can be defined. However, a large number of measurements or numerical simulations are required to accurately obtain the detection threshold for even a specific AUT and probe array configuration. An intelligent threshold selection method might be considered in the future. Further, the validations are limited to linear arrays in this paper. When the proposed method is extended to large-scale planar arrays, the mutual coupling between the AUT and the probe arrays in a very short distance might be nonnegligible which necessitates more investigations to guarantee the diagnosis accuracy in large-scale planar arrays. Furthermore, complex signal measurements are required in the method. It would be desirable to achieve the diagnosis for beamforming antenna arrays by amplitude-only measurements since phase measurements are less reliable or even non-accessible in higher frequency bands.

REFERENCES

[1] S.-Y. Lien, S.-L. Shieh, Y. Huang, B. Su, Y.-L. Hsu, and H.-Y. Wei, "5G new radio: Waveform, frame structure, multiple access, and initial access," *IEEE Communications Magazine*, vol. 55, no. 6, pp. 64–71, 2017.

[2] P. Pan, H. Wang, Z. Zhao, and W. Zhang, "How many antenna arrays are dense enough in massive MIMO systems," *IEEE Transactions on Vehicular Technology*, vol. 67, no. 4, pp. 3042–3053, 2017.

[3] J. Lee, E. M. Ferren, D. P. Woollen, and K. M. Lee, "Near-field probe used as a diagnostic tool to locate defective elements in an array antenna," *IEEE Transactions on Antennas and Propagation*, vol. 36, no. 6, pp. 884–889, 1988.

[4] S. Mano and T. Katagi, "A method for measuring amplitude and phase of each radiating element of a phased array antenna," *Electronics and Communications in Japan (Part I: Communications)*, vol. 65, no. 5, pp. 58–64, 1982.

[5] T. Takahashi, Y. Konishi, and I. Chiba, "A novel amplitude-only measurement method to determine element fields in phased arrays," *IEEE Transactions on Antennas and Propagation*, vol. 60, no. 7, pp. 3222–3230, 2012.

[6] L. Gattoufi, D. Picard, A. Rekiouak, and J. C. Bolomey, "Matrix method for near-field diagnostic techniques of phased arrays," in *Proceedings of International Symposium on Phased Array Systems and Technology*. IEEE, 1996, pp. 52–57.

[7] O. M. Bucci, M. D. Migliore, G. Panariello, and P. Sgambato, "Accurate diagnosis of conformal arrays from near-field data using the matrix method," *IEEE Transactions on Antennas and Propagation*, vol. 53, no. 3, pp. 1114–1120, 2005.

[8] H. Chen, W. Lin, S. Wang, W. Che, and Q. Xue, "A calibrated over-the-air measurement method for error vector magnitude characterization," *IEEE Transactions on Instrumentation and Measurement*, vol. 71, pp. 1–8, 2022.

[9] W. Xue, F. Li, X. Chen, S. Zhu, A. Zhang, and T. Svensson, "A unified approach for uncertainty analyses for total radiated power and total isotropic sensitivity measurements in reverberation chamber," *IEEE Transactions on Instrumentation and Measurement*, vol. 70, pp. 1–12, 2020.

[10] M. N. Hamdy, "An introduction to LTE smart base station antennas," *White Paper*, 2017.

[11] F. Athley and M. N. Johansson, "Impact of electrical and mechanical antenna tilt on LTE downlink system performance," in *2010 IEEE 71st Vehicular Technology Conference*. IEEE, 2010, pp. 1–5.

[12] M. A. Salas-Natera, R. M. Rodriguez-Osorio, and L. de Haro, "Procedure for measurement, characterization, and calibration of active antenna arrays," *IEEE Transactions on Instrumentation and Measurement*, vol. 62, no. 2, pp. 377–391, 2012.

[13] M. Salucci, A. Gelmini, G. Oliveri, and A. Massa, "Planar array diagnosis by means of an advanced Bayesian compressive processing," *IEEE Transactions on Antennas and Propagation*, vol. 66, no. 11, pp. 5892–5906, 2018.

[14] M. E. Eltayeb, T. Y. Al-Naffouri, and R. W. Heath, "Compressive sensing for millimeter wave antenna array diagnosis," *IEEE Transactions on Communications*, vol. 66, no. 6, pp. 2708–2721, 2018.

[15] M. D. Migliore, "A compressed sensing approach for array diagnosis from a small set of near-field measurements," *IEEE Transactions on Antennas and Propagation*, vol. 59, no. 6, pp. 2127–2133, 2011.

[16] K. Jeong, S. B. Choi, and H. Choi, "Sensor fault detection and isolation using a support vector machine for vehicle suspension systems," *IEEE Transactions on Vehicular Technology*, vol. 69, no. 4, pp. 3852–3863, 2020.

[17] L. Wen, X. Li, L. Gao, and Y. Zhang, "A new convolutional neural network-based data-driven fault diagnosis method," *IEEE Transactions on Industrial Electronics*, vol. 65, no. 7, pp. 5990–5998, 2017.

[18] K.-M. Chen, T.-H. Chang, K.-C. Wang, and T.-S. Lee, "Machine learning based automatic diagnosis in mobile communication networks," *IEEE Transactions on Vehicular Technology*, vol. 68, no. 10, pp. 10 081–10 093, 2019.

[19] R. Long, J. Ouyang, F. Yang, W. Han, and L. Zhou, "Multi-element phased array calibration method by solving linear equations," *IEEE Transactions on Antennas and Propagation*, vol. 65, no. 6, pp. 2931–2939, 2017.

[20] Z. Wang, F. Zhang, H. Gao, O. Franek, G. F. Pedersen, and W. Fan, "Over-the-air array calibration of mmwave phased array in beam-steering mode based on measured complex signals," *IEEE Transactions on Antennas and Propagation*, 2021.

[21] O. Franek, "Phasor alternatives to Friis' transmission equation," *IEEE Antennas and Wireless Propagation Letters*, vol. 17, no. 1, pp. 90–93, 2017.

[22] M. Li, B. G. Zhong, and S. Cheung, "Isolation enhancement for MIMO patch antennas using near-field resonators as coupling-mode transducers," *IEEE Transactions on Antennas and Propagation*, vol. 67, no. 2, pp. 755–764, 2018.

[23] Y. Zhu, Y. Chen, and S. Yang, "Decoupling and low-profile design of dual-band dual-polarized base station antennas using frequency-selective surface," *IEEE Transactions on Antennas and Propagation*, vol. 67, no. 8, pp. 5272–5281, 2019.